Int. J. Heat Mass Transfer. Vol. 34, No. 6, pp. 1347–1354, 1991
Printed in Great Britain

0017–9310/91 $3.00 + 0.00

Heat transfer and interactive buoyant vortex shedding by a pair of circular cylinders in transverse arrangement

CHANG-JOON SONG and KEUN-SHIK CHANG

Korea Advanced Institute of Science and Technology, Department of Aerospace Engineering, P.O. Box 150, Cheongryang, Seoul, Korea

(*Received* 7 *May* 1990 *and in final form* 2 *July* 1990)

Abstract—The heat transfer and fluid flow patterns in the mixed convection regimes for the double circular cylinders arranged transverse to the vertical air stream are presented. The difficulty of the non-singular grid generation for the present triply-connected region has been effectively resolved by the FEM–FDM grid blending technique which requires embedding of finite elements in the small area of major geometrical difficulty. The unsteady streamfunction values are assigned rigorously on the cylinder surfaces and on the far-field boundary. It has been found that the Karman vortex street breaks down behind the double heated cylinders in a transient manner for a certain Richardson number range due to the buoyancy effect and vortex interaction, in contrast to the sudden breakdown applicable to a single heated cylinder.

1. INTRODUCTION

A NUMBER of experimental research papers on the mixed convection heat transfer from a circular cylinder as well as from tube banks have been published. Sharma and Sukhatme [1] presented an experimental study on the mean heat transfer from a heated tube in a crossflow. Oosthuizen and Madan [2] suggested a correlation formula relating the forced convection heat transfer to the mixed convection one. They also studied the heat transfer from the circular cylinder affected by change of forced flow direction [3]. Hatton *et al.* [4] proposed in the mixed convection regime a correlation formula based on the vectorial addition of the forced and natural convection heat transfer coefficients.

Numerical studies have also been accomplished by many authors. Joshi and Sukhatme [5], Sparrow and Lee [6], and Merkin [7] analysed the mixed convection problem for a circular cylinder using the boundary layer approximation. Jain and Lohar [8] investigated unsteady mixed convection heat transfer from a circular cylinder under the Boussinesq approximation. Badr [9, 10] also calculated the Navier–Stokes and energy equations and studied the influence of the forced flow direction in the low Reynolds number range up to 40.

The mixed convection heat transfer from a circular cylinder has attracted much attention due to application to the probe of the hot-wire anemometer submerged in a low speed fluid flow. The study of the heat transfer characteristics of tube banks, on the other hand, has attracted researchers due to the importance in view of the heat exchanger design. Faghri and Rao [11] investigated the effect of fins installed at each cylinder of the tube banks. The heat and momentum transfer from the in-line tube bundles in a crossflow were studied numerically in ref. [12]. In these works the computational domain was split into smaller regions, each of which has periodic boundary conditions in one or two directions.

Noto and Matsumoto [13] showed through experiments that the Karman vortex street behind a cylinder could suddenly break down due to the buoyancy force assisting the mixed convection. For mixed convective flow parallel to the direction of the gravitational force, it was computed that by increasing the Grashof number against a constant Reynolds number the Strouhal number indeed increased gradually before it suddenly fell to zero [14].

In this paper the fluid flow and heat transfer characteristics of the unsteady mixed convection about a pair of parallel circular cylinders arranged transverse to the vertical air stream are studied. The interaction of the vortex streets from the two cylinders, which is already complicated and nonperiodic depending on the cylinder distance, was proved to be much affected by the buoyancy force. The present problem cannot be treated as a component of the tube bank system having periodic boundary conditions. Instead the whole flow domain has been computed here with the far-field boundary conditions specified accurately. Since the flow domain is also mathematically triply connected, the ordinary computational grid generation has the trouble of having grid singularity on the body surface; Chen and Tong [15], for example, could not avoid the singular points on the droplet surfaces of the droplet arrays. The present authors have introduced the FEM–FDM grid blending technique to remove the grid singularity as well as the difficulty in applying surface boundary conditions; see also ref. [16].

NOMENCLATURE

a	cylinder radius
C_D	drag coefficient, drag/$(1/2)\rho U_\infty^2(2a)$
C_L	lift coefficient, lift/$(1/2)\rho U_\infty^2(2a)$
C_p	specific heat at constant pressure
g	gravitational acceleration
g^*	dimensionless gap size between double circular cylinders
Gr	Grashof number, $g\beta(T-T_\infty)(2a)^3/\nu^2$
h	local heat transfer coefficient
k	thermal conductivity
n	normal direction from computational boundary
Nu_θ, Nu_m	local and mean Nusselt numbers
Nu_{for}	forced convection Nusselt number
Pr	Prandtl number, $\nu/\alpha = \mu C_p/k$
Re	Reynolds number, $2aU_\infty/\nu$
t	dimensionless time
T	temperature
T_w, T_∞	temperature of wall and free stream
u, v	vertical and horizontal components of velocity
U_∞	speed of free stream
x, y	Cartesian coordinates.

Greek symbols

α	thermal diffusivity
β	coefficient of volumetric thermal expansion
ζ	dimensionless vorticity
θ	angular coordinate
μ	dynamic viscosity
ν	kinematic viscosity
ξ, η	general coordinates
ρ	density
ϕ	dimensionless temperature, $(T-T_\infty)/(T_w-T_\infty)$
ψ	dimensionless streamfunction.

When the two cylinders are close within one diameter distance and when they are not heated, it has been shown that the wake flow is aperiodic and bistable [16–18]. In the present work we have shown that symmetry and periodicity can be resumed by the buoyancy force assisting the flow at the same Reynolds number. Also, contrary to the earlier findings that the Karman vortex street behind a single heated cylinder could break down very suddenly [13, 14], it has been found that an oscillating transient period of time is necessary before the vortex sheddings are broken in the case of heated interactive cylinders. We have considered three cases of Grashof number, $Gr = 10^3$, 5×10^3, and 10^4 while the Reynolds number was fixed at $Re = 100$. The Prandtl number was taken as 0.7 and the cylinder distance was 0.7 diameter.

2. PROBLEM STATEMENT AND MATHEMATICAL FORMULATION

We consider two-dimensional, unsteady incompressible viscous flow past heated double circular cylinders arranged transverse to the air stream. The schematic diagram of the flow geometry is given in Fig. 1. The direction of the incident flow is upward and the buoyancy force assists the flow. The fluid properties such as kinematic viscosity, ν, coefficient of volumetric thermal expansion, β, and thermal conductivity, k, are assumed constant. The Boussinesq approximation is taken by holding the density, ρ, constant except in the buoyancy force term.

The conservation equations of mass, momentum, and energy can be put in non-dimensional vorticity and streamfunction form as

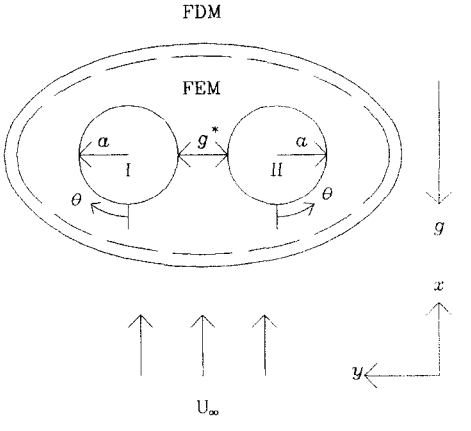

FIG. 1. Schematic diagram of the flow and division of the computational domain.

$$\frac{\partial\zeta}{\partial t}+u\frac{\partial\zeta}{\partial x}+v\frac{\partial\zeta}{\partial y}=\frac{2}{Re}\nabla^2\zeta-\frac{Gr}{2Re^2}\frac{\partial\phi}{\partial y} \tag{1}$$

$$\nabla^2\psi=-\zeta \tag{2}$$

$$\frac{\partial\phi}{\partial t}+u\frac{\partial\phi}{\partial x}+v\frac{\partial\phi}{\partial y}=\frac{2}{Re\,Pr}\nabla^2\phi \tag{3}$$

where

$$\nabla^2\equiv\frac{\partial^2}{\partial x^2}+\frac{\partial^2}{\partial y^2}$$

$$u=\frac{\partial\psi}{\partial y},\quad v=-\frac{\partial\psi}{\partial x}$$

$$Re = 2aU_\infty/\nu$$

$$Gr = g\beta(T_w - T_\infty)(2a)^3/\nu^2$$

$$Pr = \nu/\alpha = \mu C_p/k.$$

The dimensionless variables t, ζ, ψ and ϕ are defined as

$$t = t^* U_\infty/a, \quad \zeta = \zeta^* a/U_\infty$$

$$\psi = \psi^*/aU_\infty, \quad \phi = (T - T_\infty)/(T_w - T_\infty)$$

where the asterisk implies the corresponding dimensional quantity. Here T is absolute temperature.

We assume that the fluid is initially stationary before the double cylinders are suddenly heated to a unit temperature. The boundary conditions are taken as follows:

wall surface boundary

$$\psi = \psi_{\text{wall}}(t)$$

$$\frac{\partial \psi}{\partial n} = 0, \quad \phi = 1; \tag{4}$$

far-field boundary

$$\psi = \psi_{\text{far}}(t, x, y)$$

$$\zeta = \phi = 0 \text{ (inflow boundary)}$$

$$\frac{\partial \zeta}{\partial n} = \frac{\partial \phi}{\partial n} = 0 \text{ (outflow boundary)} \tag{5}$$

where n denotes the normal direction from the boundaries. The streamfunction values on both the surface and far-field boundaries are not fixed but calculated at each time step. $\psi_{\text{wall}}(t)$ can be determined from the single valuedness of pressure [19] and $\psi_{\text{far}}(t, x, y)$ is obtained using the integral-series method [20] developed in the earlier work of the authors. The far-field boundary is located from the origin by as much as 25 cylinder radii.

3. NUMERICAL METHODS

We apply the FEM–FDM grid blending technique to the present calculations. The computational domain of the present problem is split into two subdomains overlapped over a thin common buffer layer. This buffer layer belongs to either the FEM or the FDM subdomain depending upon the computation process. The newest information calculated in one subdomain is iteratively transferred to the other through this buffer layer. The buffer layer occupies as few as one element width band.

Discretizing the FEM subdomain to apply the Galerkin method leads to the following system of ordinary differential equations of matrix form:

$$\mathbf{M}\frac{d\boldsymbol{\zeta}}{dt} + \mathbf{C}(\psi)\boldsymbol{\zeta} + \frac{2}{Re}\mathbf{K}\boldsymbol{\zeta} = \frac{Gr}{2Re^2}\mathbf{B}\boldsymbol{\phi} \tag{6}$$

$$\mathbf{K}\boldsymbol{\psi} - \mathbf{M}\boldsymbol{\zeta} = 0 \tag{7}$$

$$\mathbf{M}\frac{d\boldsymbol{\phi}}{dt} + \mathbf{C}(\psi)\boldsymbol{\phi} + \frac{2}{Re\,Pr}\mathbf{K}\boldsymbol{\phi} = 0. \tag{8}$$

The Euler explicit method is used to integrate equations (6) and (8) in the time direction. The linear systems are solved with the frontal technique which is a sort of direct Gaussian elimination. Since there is no pressure term, the four-node isoparametric elements with bilinear shape functions are applied to all variables.

In order to accomplish calculations in the FDM subdomain the governing equations (1)–(3) are transformed to the general coordinate system of ξ and η. The transformation of the equations is based on the following formula:

$$f_x = (y_\eta f_\xi - y_\xi f_\eta)/J^2 \tag{9}$$

$$f_y = (x_\xi f_\eta - x_\eta f_\xi)/J^2 \tag{10}$$

$$\nabla^2 f = (\alpha f_{\xi\xi} - 2\beta f_{\xi\eta} + \gamma f_{\eta\eta} + \sigma f_\eta + \tau f_\xi)/J^2 \tag{11}$$

where

$$\alpha = x_\eta^2 + y_\eta^2 \tag{12}$$

$$\beta = x_\xi x_\eta + y_\xi y_\eta \tag{13}$$

$$\gamma = x_\xi^2 + y_\xi^2 \tag{14}$$

$$\sigma = [(\alpha x_{\xi\xi} - 2\beta x_{\xi\eta} + \gamma x_{\eta\eta})y_\xi - (\alpha y_{\xi\xi} - 2\beta y_{\xi\eta} + \gamma y_{\eta\eta})x_\xi]/J \tag{15}$$

$$\tau = [(\alpha y_{\xi\xi} - 2\beta y_{\xi\eta} + \gamma y_{\eta\eta})x_\xi - (\alpha x_{\xi\xi} - 2\beta x_{\xi\eta} + \gamma x_{\eta\eta})y_\eta]/J \tag{16}$$

$$J = x_\xi y_\eta - x_\eta y_\xi. \tag{17}$$

Here f is an arbitrary function and all subscripted variables represent derivatives. The metric coefficients and the Jacobian, J, are obtained by the numerical grid generation technique. Of the many techniques, that of Steger and Sorenson [21] is chosen in the present study to generate the O-mesh to be used in the FDM region surrounding the FEM region.

Central differencing in space and forward Euler differencing in time are used to retain compatibility with the FEM formulation. The finite difference form of the streamfunction equation is solved by the point-SOR method.

4. RESULTS AND DISCUSSION

The discretized finite elements in the inner FEM region and part of the finite difference grid in the outer FDM region are shown in Fig. 2. The finite elements and the nodal points were counted as 780 and 849, respectively, while the finite difference grid size was 61×41. It is noteworthy that the number of common elements in the buffer layer was only 60; these are marked by the shading in Fig. 2. The discretized time step Δt was 0.02 and each case of the present calculations has been accomplished within 60 s of the dimensionless time.

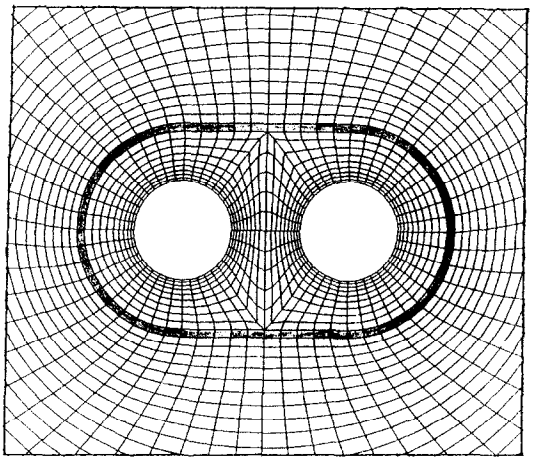

FIG. 2. The blended grid system.

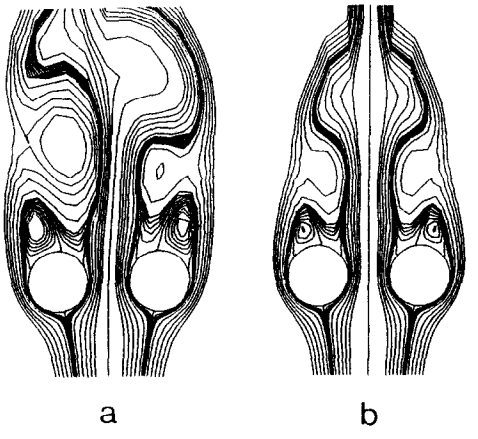

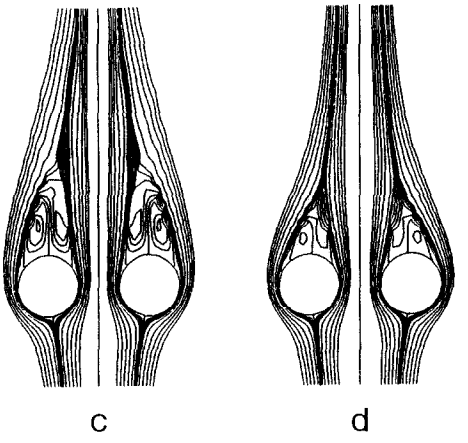

FIG. 3. Streamlines: (a) $Gr = 10^3$, $t = 60$; (b) $Gr = 5 \times 10^3$, $t = 20$; (c) $Gr = 5 \times 10^3$, $t = 60$; (d) $Gr = 10^4$, $t = 60$. ($Re = 100$ in all cases.)

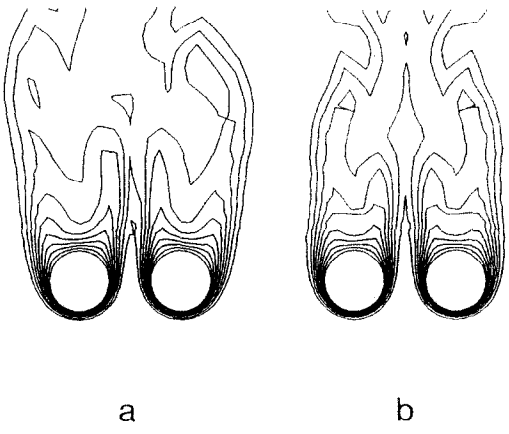

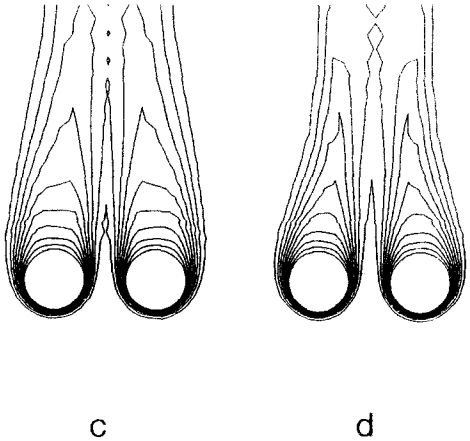

FIG. 4. Isotherms: (a) $Gr = 10^3$, $t = 60$; (b) $Gr = 5 \times 10^3$, $t = 20$; (c) $Gr = 5 \times 10^3$, $t = 60$; (d) $Gr = 10^4$, $t = 60$. ($Re = 100$ in all cases.)

It is well known that the wake flow behind a single cylinder becomes unstable and the Karman vortex street is built up if the Reynolds number is raised over 40. In the pure buoyant flow of natural convection, however, there is no Karman vortex street. Buoyancy then acts as a stabilizing force in the mixed convection regime if the free stream is in the vertical direction. Experiments by Noto and Matsumoto [13] and numerical calculations by Chang and Sa [14] have indeed shown that the Karman vortex street could suddenly break down by the buoyancy force.

However, the wake flow behind the double cylinders arranged transverse to the free stream is more unstable and show the bistability when $g^* < 1.0$. The gap flow between the two cylinders is biased to one or the other direction [16]. If the double cylinders are heated to generate the buoyancy force, the gap flow then has the tendency of straightening up. The streamlines shown in Fig. 3 describe such a behaviour. When the buoyancy force is weak, the gap flow remains still biased (see Fig. 3(a)). With stronger buoyancy force, however, the gap flow becomes straight and the whole wake flow takes first the symmetric shedding form (see Fig. 3(b)) and then the stationary twin vortices attach to the cylinders. The temperature and the vorticity contours shown in Figs. 4 and 5 also support

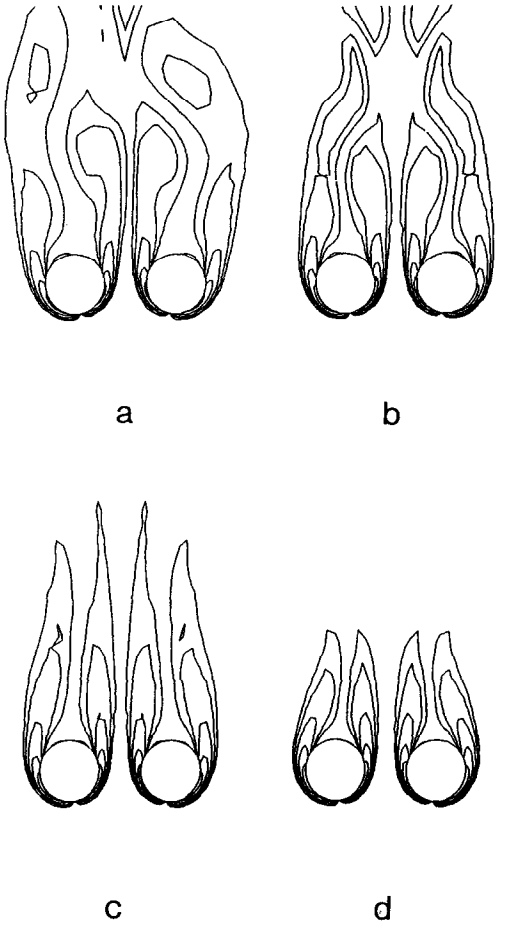

FIG. 5. Isovorticities: (a) $Gr = 10^3$, $t = 60$; (b) $Gr = 5 \times 10^3$, $t = 20$; (c) $Gr = 5 \times 10^3$, $t = 60$; (d) $Gr = 10^4$, $t = 60$. ($Re = 100$ in all cases.)

such characteristics. In contrast to the sudden vortex breakdown in the case of a single cylinder [14], the present double cylinders experience a transient vortex breakdown process. For some time after sudden heating of the cylinders in a free stream, the dynamic vortex shedding persists in a transient manner before it finally breaks down to the steady-state twin vortices. As the Richardson number, Gr/Re^2, is further increased, the transient time period is shortened to as small as zero. The lift coefficient curves shown in Fig. 6 clearly show the accelerated transient oscillatory behaviour with higher Grashof number.

Figure 7 shows the drag coefficient curves. In the case of $Gr = 10^3$, the drag coefficients of the two cylinders are seen to deviate from each other (curves I and II). The two curves are in accord with each other in the cases of $Gr = 5 \times 10^3$ and 10^4. Like the case of a single cylinder, the drag coefficient increases as the Grashof number is raised. This is because the wake becomes more and more buoyant so that the pressure drag as well as the skin friction are elevated for a fixed Reynolds number.

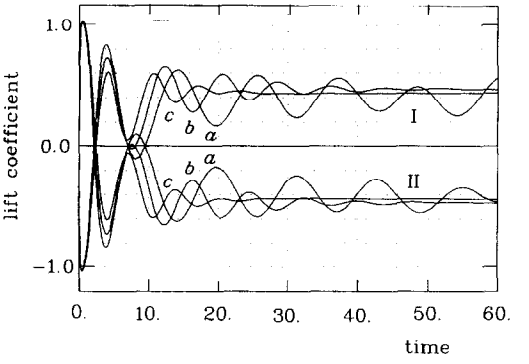

FIG. 6. The lift coefficient (C_L) curves: (a) $Gr = 10^3$; (b) $Gr = 5 \times 10^3$; (c) $Gr = 10^4$. ($Re = 100$ in all cases.)

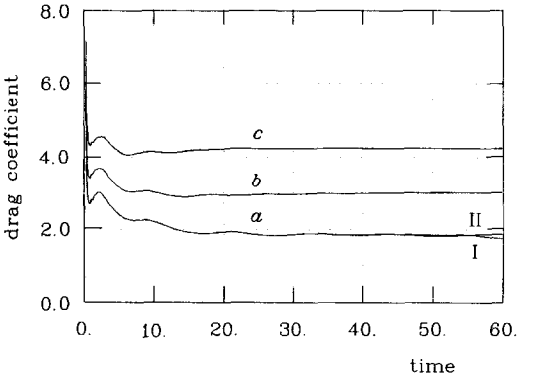

FIG. 7. The drag coefficient (C_D) curves: (a) $Gr = 10^3$; (b) $Gr = 5 \times 10^3$; (c) $Gr = 10^4$. ($Re = 100$ in all cases.)

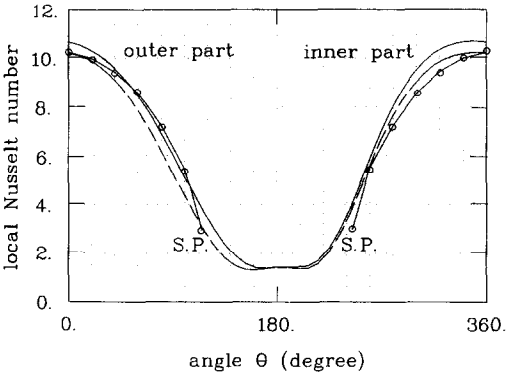

FIG. 8. The local Nusselt number distributions on one of the double cylinders: ----, $Gr = 5 \times 10^3$, $Re = 100$; ——, $Gr = 10^4$, $Re = 100$; —○—, $Gr/Re^2 = 1.0$ for a single cylinder [5]; S.P. denotes the separation point.

Figure 8 shows the distribution of the local Nusselt number defined by

$$Nu_\theta = 2ah/k = -2\left(\frac{\partial \phi}{\partial n}\right)_{\text{wall}}. \qquad (18)$$

For $Gr/Re^2 = 1.0$ ($Gr = 10^4$ and $Re = 100$), the present result is compared with the single cylinder result by Joshi and Sukhatme [5]. The two agree closer in the outer part than in the inner part on one of the

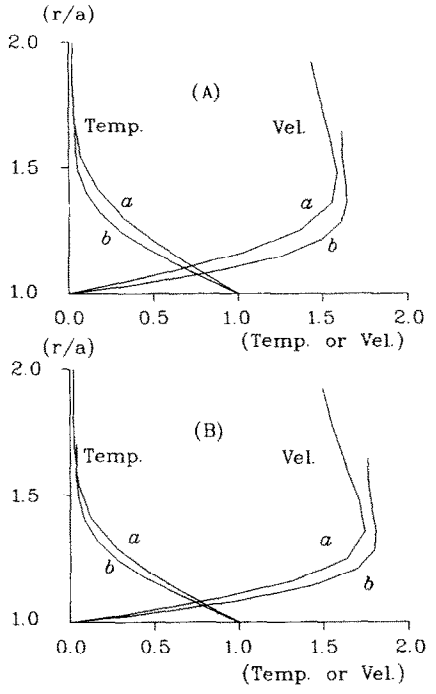

FIG. 9. The temperature and velocity profiles on the cylinder surfaces: (a) $\theta = 90°$; (b) $\theta = 270°$. (A) $Gr = 5 \times 10^3$, $Re = 100$; (B) $Gr = 10^4$, $Re = 100$.

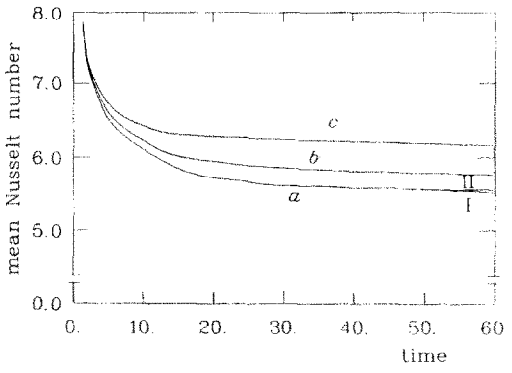

FIG. 10. The mean Nusselt number curves: (a) $Gr = 10^3$; (b) $Gr = 5 \times 10^3$; (c) $Gr = 10^4$. ($Re = 100$ in all cases.)

double cylinders since the flow of the outer part is more similar to that of a single cylinder. It implies that the thermal convection is slightly more vigorous in the inner part than in the outer part. This fact is suggested by the thinner thermal and velocity boundary layers on the inner part ($\theta = 270°$) than on the outer part ($\theta = 90°$) as plotted in Fig. 9.

Figure 10 shows the time history of the mean Nusselt number. Similar to the drag coefficient curves, the mean Nusselt number of one cylinder is increased with the Grashof number due to the enhanced thermal convection process. In Table 1 the mean Nusselt numbers of the double cylinders are compared with the single cylinder results reported by some researchers. The correlation values of Nu_m are obtained from the formula by Oosthuizen and Madan [2]

$$\frac{Nu_m}{Nu_{for}} = 1 + 0.18\left(\frac{Gr}{Re^2}\right) - 0.011\left(\frac{Gr}{Re^2}\right)^2. \quad (19)$$

The mean Nusselt numbers of the double cylinders are seen again slightly larger than those of the single cylinder cases because of the enhanced heat transfer in the inner parts of the double cylinders.

5. CONCLUSION

The mixed convective flow and heat transfer from the double circular cylinders are studied for three cases of Gr/Re^2. The FEM–FDM grid blending technique has beautifully worked for the triply-connected configuration of the present problem. It has been found that the breakdown of the Karman vortex street from the double heated cylinders occurs in a transient manner due to the vortex interaction and buoyancy effect, in contrast to the sudden breakdown applicable to the single heated cylinder. It has also been found that heat transfer is more vigorous locally on the inner parts than on the outer parts of the double cylinders due to the activated buoyant gap flow.

Table 1. Mean Nusselt numbers

Authors	Nu_{for} $Re = 100$ $Gr = 0$	Nu_m $Re = 100$ $Gr = 5.0 \times 10^3$	Nu_m $Re = 100$ $Gr = 1.0 \times 10^4$
Single cylinder			
Eckert and Soehngen [22]	5.23	5.69[b]	6.11[b]
Hilpert [23]	5.26	5.72[b]	6.15[b]
Chang and Sa [14]	5.23[a]	5.56[a]	5.98[a]
McAdams [24]	5.04	5.48[b]	5.89[b]
Double cylinders			
Present results	--	5.75[a]	6.16[a]

[a] Navier–Stokes computation value.
[b] Correlation value.

REFERENCES

1. G. K. Sharma and S. P. Sukhatme, Combined free convection heat transfer from a heated tube to a transverse air stream, *J. Heat Transfer* **91,** 457–459 (1969).
2. P. H. Oosthuizen and S. Madan, Combined convective heat transfer from horizontal cylinders in air, *J. Heat Transfer* **92,** 194–196 (1970).
3. P. H. Oosthuizen and S. Madan, The effect of flow direction on combined convective heat transfer from cylinders to air, *J. Heat Transfer* **92,** 240–242 (1970).
4. A. P. Hatton, D. D. James and H. W. Swire, Combined forced and natural convection with low-speed air flow over horizontal cylinders, *J. Fluid Mech.* **42,** 17–31 (1970).
5. N. D. Joshi and S. P. Sukhatme, An analysis of combined free and forced convection heat transfer from a horizontal circular cylinder to a transverse flow, *J. Heat Transfer* **93,** 441–448 (1971).
6. E. M. Sparrow and L. Lee, Analysis of mixed convection about a horizontal cylinder, *Int. J. Heat Mass Transfer* **19,** 229–231 (1976).
7. J. H. Merkin, Mixed convection from a horizontal circular cylinder, *Int. J. Heat Mass Transfer* **20,** 73–77 (1977).
8. P. C. Jain and B. L. Lohar, Unsteady mixed convection heat transfer from a horizontal circular cylinder, *J. Heat Transfer* **101,** 126–131 (1979).
9. H. M. Badr, Laminar combined convection from a horizontal cylinder—parallel and contra flow regimes, *Int. J. Heat Mass Transfer* **27,** 15–27 (1984).
10. H. M. Badr, On the effect of flow direction on mixed convection from a horizontal cylinder, *Int. J. Numer. Meth. Fluids* **5,** 1–12 (1985).
11. M. Faghri and N. Rao, Numerical computation of flow and heat transfer in finned and unfinned tube banks, *Int. J. Heat Mass Transfer* **30,** 363–372 (1987).
12. Y. Chang, A. N. Beris and E. E. Michaelides, A numerical study of heat and momentum transfer for tube bundles in crossflow, *Int. J. Numer. Meth. Fluids* **9,** 1381–1394 (1989).
13. K. Noto and R. Matsumoto, A breakdown of the Karman vortex street due to the natural convection. In *Flow Visualization III*, p. 348. Springer, Berlin (1985).
14. K. S. Chang and J. Y. Sa, The effect of buoyancy on vortex shedding in the near-wake behind a circular cylinder, *J. Fluid Mech.* **220,** 253–266 (1990).
15. S. J. Chen and A. Y. Tong, Application of elliptic grid generation technique to the solution of hydrodynamics and heat transfer of droplet arrays at intermediate Reynolds numbers, *Int. J. Heat Mass Transfer* **31,** 1063–1072 (1988).
16. K. S. Chang and C. J. Song, Interactive vortex shedding from a pair of circular cylinders in transverse arrangement, *Int. J. Numer. Meth. Fluids* **11,** 317–329 (1990).
17. C. H. K. Williamson, Evolution of a single wake behind a pair of bluff bodies, *J. Fluid Mech.* **159,** 1–18 (1985).
18. H. J. Kim and P. A. Durbin, Investigation of the flow between a pair of circular cylinders in the flopping regime, *J. Fluid Mech.* **196,** 431–448 (1988).
19. S. K. Park, K. S. Chang and C. E. Park, Interactive laminar natural convection from a pair of horizontally parallel square cylinders, *Proc. 1st Computational Fluid Dynamics Symp.*, pp. 445–448. Chuo University Tokyo, Japan (1987).
20. J. Y. Sa and K. S. Chang, On far-field stream function condition for two dimensional incompressible flows, *J. Computational Phys.* **91**(2), 398–412 (1990).
21. J. R. Steger and R. L. Sorenson, Automatic mesh-point clustering near a boundary in grid generation with elliptic partial differential equation, *J. Computational Phys.* **33,** 405–410 (1979).
22. E. R. G. Eckert and E. Soehngen, Distribution of heat transfer coefficients around circular cylinder in cross flow at Reynolds numbers 20 to 500, *Trans. ASME* **74,** 343–347 (1952).
23. R. Hilpert, *Forsch. Geb. IngWes.* **4,** 215 (1933).
24. W. H. McAdams, *Heat Transmission.* McGraw-Hill, New York (1954).

TRANSFERT DE CHALEUR ET DEVELOPPEMENT D'UN VORTEX LIBRE PAR UNE PAIRE DE CYLINDRES CIRCULAIRES DANS UN ARRANGEMENT TRANSVERSAL

Résumé—On présente le transfert de chaleur et les configurations d'écoulement dans des régimes de convection mixtes pour deux cylindres circulaires en arrangement transversal à un écoulement d'air vertical. Une difficulté de génération de grille pour la région triplement connectée a été efficacement résolue par la technique mélée de grille FEM–FDM qui demande le logement des éléments finis dans une petite surface de grande difficulté géométrique. Les valeurs variables de la fonction de courant sont rigoureusement assignées sur les surfaces des cylindres et sur la frontière lointaine du domaine. On a trouvé que l'allée de tourbillons de Von Karman se rompt derrière les deux cylindres chauffés d'une façon variable, pour un certain domaine de nombre de Richardson due à un effet de flottement et une interaction de tourbillons, en contraste avec la rupture nette dans le cas d'un cylindre chaud unique.

WÄRMEÜBERGANG UND AUFTRIEBSBEDINGTE WIRBELABLÖSUNG AN EINEM PAAR QUERLIEGENDER KREISZYLINDER

Zusammenfassung—Es werden die Formen von Wärmeübergang und Strömung bei Mischkonvektion an einem Paar von Kreiszylindern, das quer von Luft angeströmt wird, vorgestellt. Die Schwierigkeit der nicht-singulären Gittergenerierung wird für das vorliegende dreifach verbundene Gebiet mit Hilfe des FEM–FDM-Verfahrens der Gittererzeugung bewältigt. Dieses Verfahren erfordert die Einbettung zusätzlicher Elemente in dem kleinen, geometrisch schwierigen Gebiet. Die nicht-stationären Werte der Stromfunktion werden exakt an den Zylinderoberflächen und an den Begrenzungen des Fernfeldes bezeichnet. Es zeigt sich, daß die Karman'sche Wirbelstraße hinter dem beheizten Zylinderpaar in transienter Weise in einem bestimmten Bereich der Richardson-Zahl zusammenbricht. Dies wird durch Auftriebseffekte und Wirbelüberlagerung verursacht und steht im Gegensatz zum plötzlichen Zusammenbrechen bei einem einzelnen beheizten Zylinder.

ТЕПЛОПЕРЕНОС, ВЗАИМОДЕЙСТВИЕ И СРЫВ КОНВЕКТИВНЫХ ВИХРЕЙ ЗА ПАРОЙ ГОРИЗОНТАЛЬНЫХ ЦИЛИНДРОВ КРУГЛОГО СЕЧЕНИЯ

Аннотация—Описываются картины смешанноконвективных теплопереноса и течения жидкости в случае поперечного обтекания воздухом пары горизонтальных цилиндров круглого сечения. Трудность создания несингулярной сетки для исследуемой области с тройной связью успешно преодолена с использованием метода, сочетающего сетки МКЭ и МКР и требующего ввода конечных элементов в малую область, представляющую основную геометрическую сложность. На поверхностях цилиндров и границе удаленного поля задавались нестационарные значения функции тока. Найдено, что при некоторых значениях числа Ричардсона благодаря эффектам подъемной силы и взаимодействию вихрей происходит неустановившийся процесс разрушения вихревых дорожек Кармана за парой нагретых цилиндров, что отличается от случая с единичным цилиндром, в котором разрушение происходит внезапно.